PERGAMON International Journal of Multiphase Flow 24 (1998) 1245–1263

International Journal of Multiphase Flow

Critical heat flux and turbulent mixing in hexagonal tight rod bundles

X. Cheng *, U. Müller

Institute for Applied Thermo- and Fluiddynamics, Research Center Karlsruhe, Postfach 3640, D-76021 Karlsruhe, Germany

Received 21 January 1997; received in revised form 2 May 1998

Abstract

Experimental and theoretical investigations have been performed on critical heat flux (*CHF*) and turbulent mixing in tight, hexagonal, 7-rod bundles. Freon-12 was used as working fluid due to its low latent heat, low critical pressure and well known properties. It has been found that the two-phase mixing coefficient depends mainly on mass flux. It increases with decreasing mass flux and ranges from 0.01 to 0.04 for the test conditions considered. More than 900 *CHF* data points have been obtained in a large range of parameters: pressure 1.0–3.0 MPa and mass flux 1.0–6.0 Mg/m^2s. The effect of different parameters on *CHF* has been analysed. It has been found that the effect of pressure, mass flux and vapour quality on *CHF* is similar to that observed in circular tubes. Nevertheless, the *CHF* in the tight rod bundle is much lower than that in a circular tube of the same equivalent hydraulic diameters. The effect of wire wraps on *CHF* is mainly dependent on local vapour qualities and subsequently on flow regimes. Based on subchannel flow conditions, the effect of radial power distribution on *CHF* is small. Comparison of the test results with *CHF* prediction methods underlines the need for further work.
© 1998 Elsevier Science Ltd. All rights reserved.

Keywords: Critical heat flux; Turbulent mixing; Tight rod bundle

1. Introduction

The critical heat flux (*CHF*) is the heat flux at which boiling crisis occurs and heat transfer rate deteriorates suddenly. In a system where the heat flux is controlled, e.g. nuclear reactors, an abrupt rise of the heated wall temperature will take place. This point is clearly of crucial importance because the temperature rise may be two or three orders of magnitude, which most

* Corresponding author. Tel.: 497247 82 4897; Fax: 49 7247 82 4837; E-mail: xu.cheng@iatf.fzk.de

0301-9322/98/$19.00 © 1998 Elsevier Science Ltd. All rights reserved.
PII: S0301-9322(98)00027-5

likely will cause a failure of the heated surface. In spite of a great quantity of experimental and theoretical studies, knowledge of the precise nature of *CHF* is still incomplete. This is mainly due to the very complex nature of the two-phase flow with heat transfer (Katto, 1994).

The great importance of the *CHF*, coupled with the absence of reliable theoretical methods, led to a large number of prediction methods which can be divided into three groups: semi-empirical models, empirical correlations and look-up tables. Extensive research work has been made on modelling the relevant physical processes leading to boiling crisis (Tong and Hewitt, 1972; Weisman and Ying, 1985; Hewitt and Govan, 1990). However, many of the published *CHF* models have been based on postulated mechanisms and need to be verified for rod bundle geometries. For technical designs, empirical correlations are used which have been developed by correlating the available *CHF* database obtained from particular rod bundles and parameter ranges. The application of such correlations is only restricted to the parameter ranges considered. An extrapolation of their application to parameters out of this range could result in a large uncertainty. One of the methods to standardize empirical correlations is the *CHF* look-up table. For the circular tube geometry, large efforts have been made to develop *CHF* look-up tables (Groeneveld et al., 1996). Groeneveld et al. (1986) suggested to extend the application of the look-up table to the rod bundle geometry by introducing correction factors which have been derived empirically. However, it has been found (Cheng et al., 1997) that even for circular tube geometries, the effect of geometrical parameters, e.g. tube diameter, on *CHF* is still not sufficiently reproduced by the correction factor given.

It became evident that, due to the deficiency in understanding the boiling crisis mechanism, experimental investigations on *CHF* should be performed for each specific design of engineering equipment. Validated prediction methods for the design condition must be derived. In the last few years, interest has risen in developing tight-lattice pressurized water reactors (Oldekop et al., 1982). A detailed literature survey has indicated that experimental as well as theoretical works on *CHF* for tight hexagonal rod bundles under high pressures and high mass fluxes are scarce.

Due to technical restrictions, *CHF* experiments can only be performed in rod bundles with much fewer rods than in an original fuel bundle. The possible non-uniform distribution of heat generation and the cold-wall effect in such a small bundle could result in a significant thermal imbalance between subchannels. The flow condition in subchannels usually cannot be determined experimentally and should be obtained by using a subchannel analysis code. Therefore, a reliable subchannel analysis code is a necessary basis for analysing the *CHF* results in rod bundles. It is well known that some physical models used in subchannel analysis codes, e.g. the turbulent mixing model, affect the calculated subchannel flow condition significantly. Although a great quantity of experimental and theoretical works have been performed in the last decades on subchannel analysis, including turbulent mixing, sufficient knowledge about two-phase turbulent mixing under high pressure conditions in tight rod bundles is still not available (Wolf et al., 1987). Any information leading to a better understanding of turbulent mixing will be an important contribution for the calculation of the subchannel flow condition and the evaluation of *CHF* results in rod bundle geometries.

A program of experimental and analytical investigations on critical heat flux and turbulent mixing in hexagonal tight rod bundles has been performed at the Research Center Karlsruhe. Freon-12 was used as the working fluid due to its low latent heat, low critical pressure and well

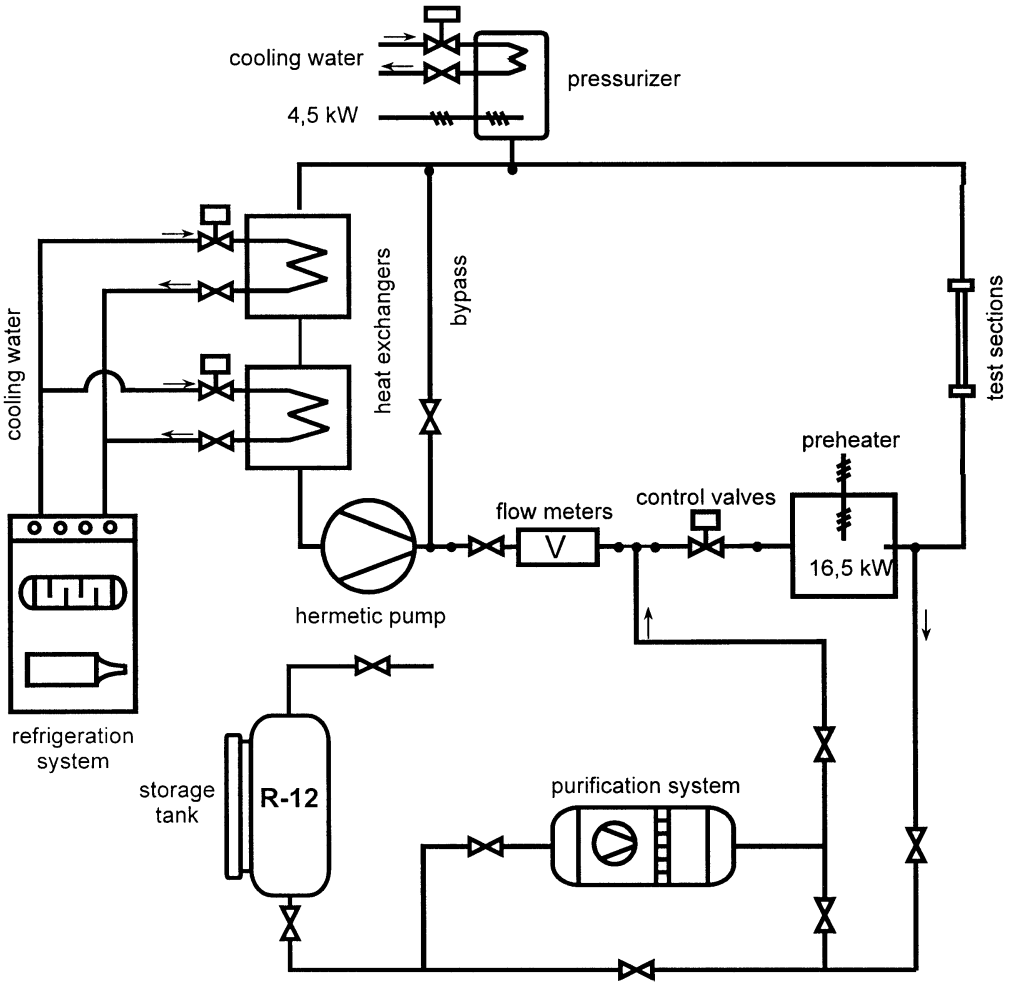

Fig. 1. Schematic diagram of the test loop.

known properties. The main objectives of the present work are to supplement the *CHF* database available for rod bundles, especially for tight rod bundles, to analyse the effect of different parameters, e.g. wire wraps on *CHF*, to identify the differences in rod bundle geometries and in circular tubes, to assess available *CHF* prediction methods and finally to investigate turbulent mixing in tight rod bundles.

2. Experimental apparatus

2.1. Test facility

The test loop used for the present study is schematically shown in Fig. 1. It consists mainly of a storage tank, a purification system, a refrigeration system, a hermetically sealed pump, a

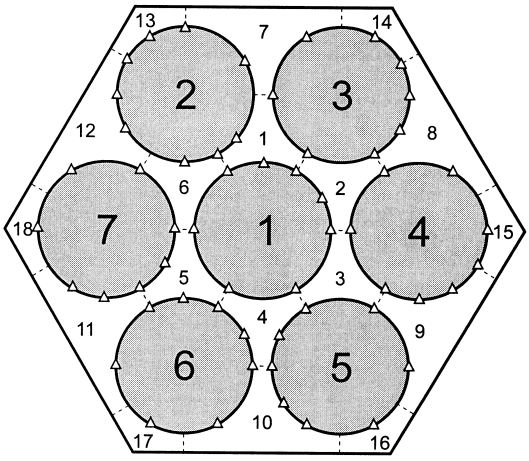

Fig. 2. Cross-section of the 7-rod bundle (Δ thermocouples).

preheater, a pressurizer, two heat exchangers, and the test section. The test loop was constructed for pressure up to 3.5 MPa. The total length of the 7-rod bundle test section is 1.24 m of which 0.6 m is heated with an axially uniform power distribution. Two bundles with different spacers (grid spacer and wire wrap) were used. To minimize the influence of the grid spacer on *CHF*, the closest upstream grid spacer was positioned 270 mm upstream from the end of the heated length. This distance is more than 60 times the bundle hydraulic diameter, so that the influence of the grid spacer on *CHF* is negligible, compared to a bare bundle (Groeneveld et al., 1986). The effect of the wire wrap on *CHF* can, therefore, be analysed by a comparison of the gridded with the wire wrapped case. In the bundle with wire wraps, the axial wire lead is 190 mm, 20 times the rod diameter.

Figure 2 shows the cross section of the 7-rod bundle. The rod diameter and the pitch are 9.5 and 10.9 mm, respectively. The rod-to-wall clearance is the same as the rod-to-rod gap, i.e. 1.4 mm. The fuel rod simulators are electrically, indirectly heated and have a uniform axial heat flux. To detect the *CHF* occurrence, thermocouples (0.5 mm o.d.) are embedded in grooves inside the cladding. A plasma spraying process and a subsequent polishing provides a smooth outer surface to the cladding. Eight thermocouples were installed in each of the rods, as indicated in Fig. 2. The junctions were located about 15 mm upstream from the end of the heated length. At the same elevation, the fluid temperatures in different subchannels are measured by using thermocouples of 0.25 mm diameter. These test data will contribute to a better understanding of turbulent mixing between subchannels. More details of the 7-rod bundle test section and the instrumentation have been documented by Cheng (1991).

The entire flow area is devided into 18 subchannels, i.e. six central subchannels, six wall subchannels and six corner subchannels. The number of the rods and the subchannels are indicated in Fig. 2. The geometric parameters of both the gridded and the wire wrapped rod bundles and of the subchannels are summarized in Table 1.

Here, d_h is the hydraulic diameter and A the flow area. It is seen that the total flow area of the six central subchannels is less than 30% of the entire bundle flow area. It is expected that about two-thirds of the bundle flow rate pass the wall region of the test section. The enthalpy

Table 1
Geometric parameters

	Central subchannel	Wall subchannel	Corner subchannel	Rod bundle
d_h mm	4.29	4.89	3.32	4.36
A, mm^2	16.01	31.59	10.02	345.7

gain in the central subchannel could be much higher than that in the wall region. It is evident that due to the strong thermal imbalance, turbulent mixing plays an important role for the enthalpy distribution in the rod bundle.

2.2. Test procedure

Before experiments, Freon-12 from the storage tank is circulated through the purification system until a high purity is obtained. The purified fluid then fills the test loop. The cooling water (glycolic water) provided by the refrigeration system flows through both heat exchangers and cools down the Freon-12 in the test loop. The pressure in the test loop is elevated by turning on the heater which is located in the lower part of the pressurizer and immersed in liquid Freon-12. After the pressure in the test loop reaches a certain level, the pump is put into operation. The required value of the fluid temperature at the test channel inlet is obtained by controlling the heating power of the preheater. The pressurizer maintains the pressure at the channel outlet so it stays constant and stable. The mass flow rate is adjusted by means of the control valve.

Experiments are performed by holding the test section outlet pressure, inlet temperature and mass flow rate constant, while the heating power is increased rapidly at first, to about 80% of the critical value and then slowly and stepwise. The time interval between power steps is long enough, so that any transient effect can be excluded. After each step of power rise, flow parameters must be adjusted again to their prescribed values. The power supply is shut-off automatically when one of the measured wall temperatures exceeds the given limiting values (e.g. 120°C). Test parameters at the last 120 s before the shut-down of the power supply are recorded by an on-line data processing system which registers up to 256 separate channels with a maximum processing frequency of 50 kHz for the total data acquisition rate.

2.3. Test parameters

The pressure is varied from 1.0 MPa up to 3.0 MPa. The maximum ratio of the system pressure to the critical pressure is about 0.75 which is higher than values used in nuclear reactors. The lower limit of the system pressure is determined by the capacity of the test facility. With the refrigerating system used, Freon-12 can be cooled down to about −10°C. To obtain a sufficiently large subcooling at the test channel inlet, the minimum pressure in the present work is 1.0 MPa. The bundle mass flux varies in the range from 1.0 to 6.0 Mg/m^{2}s. According to the scaling law of Courtaud et al. (1988), the equivalent mass flux in water ranges up to 8.5 Mg/m^{2}s. It covers a wide spectrum of technical applications and the most important range considered in *CHF* prediction methods available.

The heated length of 600 mm is selected based on the following considerations: the critical heat flux is often assumed to only be dependent on the local flow conditions, especially in the low vapour quality region. For circular tube geometries, it has been found that the influence of the heated length on *CHF* is negligible when the ratio of heated length to hydraulic diameter exceeds a limit value, e.g. 20 (Doroshchuk et al., 1975). Recently, contradictory results have been obtained by different authors concerning the effect of heated length on *CHF* (Katto and Yokoya, 1987). The experimental investigations of Müller–Menzel and Zeggel (1987) and of Cheng et al. (1997) in Freon-12 and in tubes of 4.2 and 4.6 mm inner diameter showed, however, that the effect of heated length on *CHF* is negligibly small, when the length-to-diameter ratio exceeds the value of about 85. In both experiments, the test parameters (pressure, mass flux) are very similar to that in the present 7-rod bundles. For rod bundle geometries, the effect of the heated length on *CHF* was less investigated. With the heated length of 600 mm, the ratio of heated length to hydraulic diameter of the bundle is about 140. Therefore, the influence of the heated length on *CHF* could be neglected. Moreover, with the selected heated length, it is expected that, for as many test points as possible, the exit vapour quality will fall into the range from −0.2 to +0.2, which is of interest for nuclear reactor applications.

Ten different radial power distributions have been realized, as summarized in Table 2, to study the effect of the power distribution on subchannel flow conditions and subsequently on *CHF*. The power factor of each individual rod i is defined as:

$$f_{Q,i} = \frac{7Q_i}{\sum_{j=1}^{7} Q_j}. \tag{1}$$

Where Q is the heating power. Experiments with non-uniform power distributions also provide a useful database for validating subchannel analysis codes. In cases with unheated rods, e.g. P7, the average fluid temperature in the wall subchannel no. 7 can be obtained by using the fluid temperature measured in the subchannel center and the temperatures measured on the surface of rods no. 2 and 3. By comparing the measured average fluid temperature in

Table 2
Power factor $f_{Q,i}$ of each rod

Cases	Rod 1	Rod 2	Rod 3	Rod 4	Rod 5	Rod 6	Rod 7
P1	1.0	1.0	1.0	1.0	1.0	1.0	1.0
P2	1.30	0.95	0.95	0.95	0.95	0.95	0.95
P3	1.48	0.92	0.92	0.92	0.92	0.92	0.92
P4	0.76	1.04	1.04	1.04	1.04	1.04	1.04
P5	1.17	1.17	0.0	1.17	1.17	1.17	1.17
P6	1.4	0.0	0.0	1.4	1.4	1.4	1.4
P7	2.3	0.0	0.0	0.0	2.3	2.3	0.0
P8	0.0	1.17	1.17	1.17	1.17	1.17	1.17
P9	7.0	0.0	0.0	0.0	0.0	0.0	0.0
P10	0.0	0.0	0.0	0.0	3.5	3.5	0.0

subchannels with the calculated values, empirical models in subchannel analysis codes, especially the mixing turbulent model, can be evaluated.

For each test run, errors of different parameters are analysed. The error sources consist mainly of measuring instruments, fluctuation of measured parameters, magnitude of the last power step and geometry of the test bundle. Table 3 shows typical experimental errors. Where P is the pressure, G the bundle mass flux, X_{in} the inlet vapour quality and X_{ex} the exit vapour quality. In this example, the maximum error of the measured CHF is about 2.0%. A detailed analysis shows that, for all test points, the maximum error of the measured CHF is less than 3.5%.

3. Subchannel analysis and *CHF* prediction methods

The analysis of CHF results in rod bundles requires the knowledge of the subchannel flow conditions which cannot be directly obtained experimentally. Therefore, in the present work, the subchannel analysis code COBRA-IV is used to calculate the subchannel flow conditions. Details about the COBRA-IV code and some physical models used were documented by Wheeler et al. (1976) and Cheng (1991). In the following, the empirical models for calculating single phase presure drop and turbulent mixing, which have also been experimentally investigated in the present work, are presented.

Empirical constitutive relationships are needed to calculate the pressure drop arising from friction as the fluid flows past the flow channel as well as from the drag induced by spacers. The bundle friction factors of single phase flow was determined experimentally (Cheng, 1991) and can be computed from

$$f = \frac{0.354}{Re^{0.25}} \tag{2}$$

for the bare 7-rod bundle and from

$$f = \frac{0.20}{Re^{0.18}} \tag{3}$$

for the rod bundle with wire wraps, where Re is the Reynolds number. The pressure loss induced by grid spacers is calculated by the following equation which was suggested by

Table 3
Example of typical experimental errors

	P, MPa	G, kg/m^{2}s	X_{in}	X_{ex}	CHF, kW/m^2
Measured value	2.72	3799.6	−0.24	−0.05	160.7
Maximum error	0.023	51.1	0.02	0.03	3.45

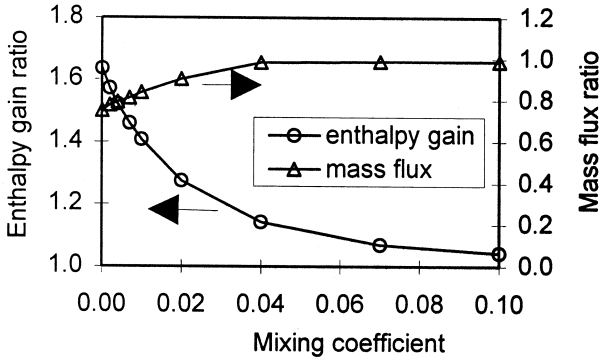

Fig. 3. Calculated enthalpy gain ratio and mass flux ratio vs the mixing coefficient.

Rehme (1973):

$$\zeta = C\left(\frac{A_k}{A_s}\right)^2. \tag{4}$$

Here A_k is the projected area of a grid spacer in the subchannel and A_s the flow area of the subchannel considered. The coefficient C was determined experimentally and was equal to 7.0.

The interchange of mass, energy and momentum between subchannels, known as mixing, arises from different mechanisms of which the most important one is turbulent mixing. In the COBRA-IV code it is assumed that turbulent mixing causes only exchange of enthalpy between neighbouring subchannels but does not result in a net mass flow[1] The transverse heat flux between two subchannels $q'_{i,j}$ due to turbulent mixing is presented as

$$q'_{i,j} = \beta\overline{G_{i,j}}(h_i - h_j), \tag{5}$$

where β is the so-called mixing coefficient, $G_{i,j}$ the axial mass flux averaged over the two subchannels considered and h the specific enthalpy. Intensive research works have been performed in the last several decades for modelling the mixing coefficient (Todreas and Rogers, 1976; Rowe and Johnson, 1974; Wolf et al., 1987). Nevertheless, experimentally verified models of the two-phase mixing coefficient under high pressure conditions in tight rod bundles are not available up to now. It is well known that the mixing coefficient depends on flow conditions as well as on subchannel geometries. Rogers and Rosehart (1972) gave the following equation for the single-phase mixing coefficient in a hexagonal rod bundle:

$$\beta = 0.0018 \cdot \frac{d_h d_r^{0.4}}{s^{1.4}} Re^{-0.1}, \tag{6}$$

where d_r is the rod diameter and s the gap width between subchannels. According to Eq. (6) the single phase mixing coefficient is about 0.005 for the test conditions considered in the

[1] A more adequate turbulent mixing based on equal volumetric-exchange is recently recommended in the literature for two-phase flow. In the COBRA-IV code, however, the equal mass-exchange turbulent mixing is still assumed for single phase flow as well as for two-phase flow.

present work. Moreover, it is expected that the two-phase mixing coefficient is larger than the single-phase coefficient. A sensitivity study of the subchannel flow condition to the constitutive equations used was performed. It has been found that, for the rod bundle with grid spacers, the model of turbulent mixing has the strongest influence on the subchannel conditions. Fig. 3 shows the ratio of the enthalpy gain and of the mass flux in the hot subchannel to the bundle average values in the gridded bundle with uniform power distribution. The enthalpy gain is defined as the difference between the outlet and the inlet enthalpy. It is seen that the enthalpy gain in the hot subchannel is higher and that the mass flux is lower than the bundle average values. Lower values of β result in a higher enthalpy gain and a lower mass flux in the hot subchannel. Increasing the β value leads to both the enthalpy gain and the mass flux in the hot subchannel approaching the bundle average conditions. It is evident that accurate knowledge of the mixing coefficient is needed to determine the subchannel flow condition and subsequently to analyse critical heat flux.

In rod bundle geometries *CHF* results can be presented either in terms of the subchannel flow condition or the bundle average condition. For a better understanding of the physical mechanisms leading to the boiling crisis, the use of the subchannel condition is more favorable, especially in small rod bundles where strong thermal imbalance appears. Table 4 summarizes four prediction methods selected in the present work to show to what extent they can reproduce the test results. The EPRI-1 correlation (Fighetti and Reddy, 1983) has been developed for square LWR lattices using more than 5000 test points from 20 different rod bundles. The KfK-3 correlation of Dalle Donne (1991) consists of two different sets of equations valid for gridded bundles and for wire wrapped bundles, respectively. It has been derived on the basis of the WSC-2 correlation (Bowring, 1979) using test data obtained in hexagonal tight lattices. The GSM.6 correlation of Courtaud et al. (1988) has been developed using the test data obtained in tight hexagonal 19-rod bundles with both Freon-12 and water. The parameter ranges given in Table 4 are valid for Freon-12 conditions. The *CHF* look-up table of Groeneveld et al. (1996) was originally developed for circular tube geometries. Nevertheless, it was suggested to extend the application of the look-up table to rod bundle geometries by using subchannel flow conditions and the correction factors introduced by the authors of the table (Groeneveld et al., 1986).

Except for the GSM.6 correlation all the prediction methods of Table 4 are derived for water conditions. To compare these prediction methods with the experimental data in Freon-12 fluid-to-fluid scaling laws are needed. To transfer the test data from Freon-12 into water-equivalent conditions, the scaling law of Courtaud et al. (1988), which was derived for water and Freon-12 in tight rod bundles, has been used.

Table 4
CHF prediction methods and their valid parameter ranges

	Fluid	P, MPa	G, Mg/m^{2}s	X_{ex}	Spacers
EPRI-1	water	0.4–17.0	0.3–5.5	−0.25–0.75	grid
KfK-3	water	2.7–14.0	≤ 5.4	−0.44–0.96	grid, wire
GSM.6	water/R12	1.2–2.9	2.0–9.0	−0.20–0.40	grid
Look-up table	water	0.1–20.0	0.0–8.0	−0.5–1.0	

4. Results and discussion

4.1. Turbulent mixing

Some experimental runs obtained in the bundle with grid spacers have been analysed in relation to turbulent mixing. To evaluate the mixing coefficient, the fluid temperature in subchannels has been measured and compared with the results calculated with the COBRA-IV code using different values of the mixing coefficient. To minimize the error of the measured fluid temperature in the subchannel considered, only experiments which satisfy the following conditions have been selected:

1. all rods whose surface bounds this subchannel are not heated. The average fluid temperature in the subchannel is obtained by using the fluid temperature measured in the subchannel center and the temperatures measured on the surfaces bounding the subchannel;
2. the measured temperatures of the fluid in the subchannel and of the surfaces bounding it do not exceed the saturation temperature over the entire experimental run, so that the presence of vapour in the subchannel and its effect on the temperature measurement can be excluded;
3. the increase in fluid temperature in the subchannel is larger than 1°C, so that the uncertainty resulting from the measurement error is kept small.

Table 5 summarizes some measured subchannel fluid temperatures: P is the bundle outlet pressure, G the bundle average mass flux, T_{in} the fluid temperature at the inlet cross-section and Q the heating power of the bundle.

Figure 4 shows the enthalpy ratio for subchannel no. 8 in the gridded bundle with four unheated rods (P7 in Table 2) at different inlet fluid temperatures. The enthalpy ratio is defined as the ratio of the calculated enthalpy rise to the measured enthalpy rise in the subchannel considered. The enthalpy ratio is plotted vs the mixing coefficient which is varied from 0.004 to 0.06. The mixing coefficient at which the enthalpy ratio is equal to unity is taken as the correct value for the condition concerned. It is seen that the mixing coefficient is only slightly affected by the fluid inlet temperature.

Figure 5(a) and (b) present the enthalpy ratio of subchannels no. 7 and 8 vs the mixing coefficient at different mass fluxes in the gridded bundle with non-uniform power distribution P7. The inlet temperature is about 10°C.

It is clearly seen that the mixing coefficient depends strongly on mass flux. The mixing coefficient decreases from about 0.04 down to 0.013, when the mass flux increases from 1–6 Mg/m^2s. Qualitatively similar results have also been obtained for different subchannels under different test conditions. A detailed analysis shows that for most test points the mixing coefficient increases with decreasing mass flux and ranges from 0.01 to 0.04. Nevertheless, an equation describing the dependence of mixing coefficient on flow conditions cannot be established due to the scattering of the test data and, especially, due to the unknown local flow condition in the subchannels. Therefore, in the following, a constant reference value of the mixing coefficient 0.02 is selected for calculating the subchannel flow condition and for evaluating CHF results. The error in local flow conditions resulting from the uncertainty in the mixing coefficient can be estimated by using the COBRA-IV code, as shown in Fig. 3. It should

Table 5
Measured fluid temperature in subchannels

Power distribution	P(MPa)	G(Mg/m^{2}s)	Tin (°C)	Q(kW)	Fluid temperature in subchannels (°C) No. 1	No. 2	No. 7	No. 8
P6	1.78	979.0	−2.6	15.03	—	—	14.8	—
P6	1.77	995.9	30.9	12.64	—	—	43.8	—
P6	1.77	2994.2	−2.0	29.96	—	—	5.3	—
P6	1.77	3002.6	29.1	21.82	—	—	33.8	—
P6	1.77	4000.2	1.3	35.11	—	—	7.5	—
P6	1.77	3988.9	22.7	27.18	—	—	26.8	—
P7	1.77	983.0	−1.1	11.90	—	—	10.5	18.6
P7	1.79	988.5	19.3	10.39	—	—	29.1	35.6
P7	1.77	2979.8	−1.0	17.84	—	—	2.8	3.6
P7	1.79	2982.8	20.8	14.27	—	—	22.8	23.8
P7	1.77	4003.9	1.2	21.21	—	—	4.6	4.9
P7	1.79	3989.1	22.9	16.19	—	—	24.4	25.5
P9	1.77	1002.7	−4.7	5.80	—	—	12.8	—
P9	1.77	2993.1	−0.9	8.97	—	—	4.2	—
P9	1.78	4007.7	0.7	10.20	—	—	5.0	—
P10	1.78	989.7	10.2	8.06	18.7	24.9	—	16.1
P10	1.76	2987.4	−0.3	14.75	2.6	5.2	—	0.9
P10	1.77	3992.4	−0.7	17.35	1.5	3.7	—	0.3

be emphasized that the quantitative conclusions achieved in the following analysis are based on the assumption of a constant mixing coefficient of 0.02.

4.2. Critical heat flux

More than 900 *CHF* data points have been obtained in a large range of parameters: pressure 1.0–3.0 MPa and mass flux 1.0–6.0 Mg/m^{2}s. Table 6 summarizes some experimental *CHF*

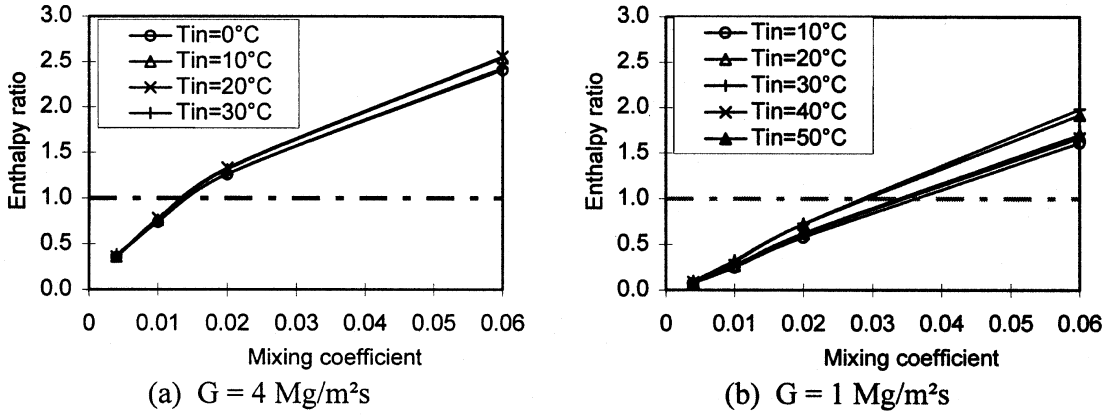

Fig. 4. Enthalpy ratio of subchannel no. 8 in the gridded bundle with the power distribution P7: (a) $G = 4$ Mg/m^{2}s; (b) $G = 1$ Mg/m^{2}s.

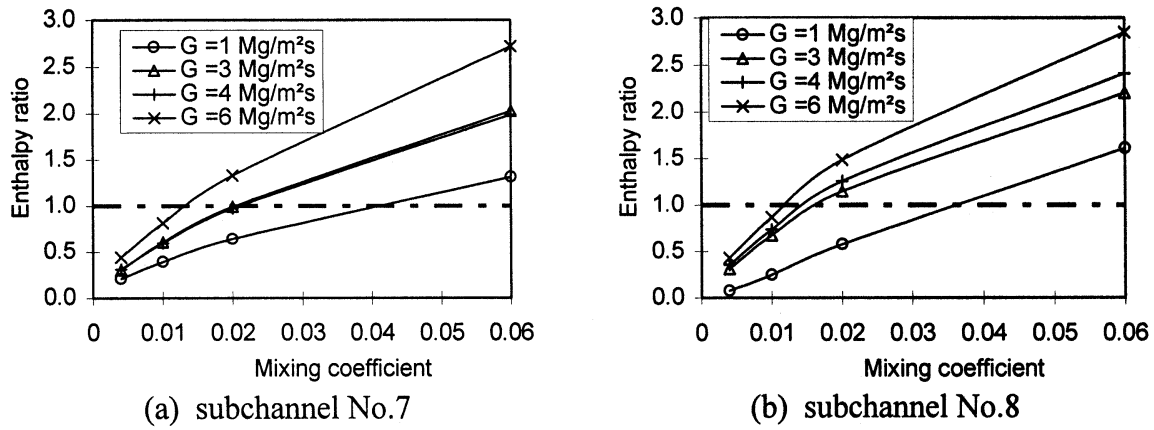

Fig. 5. Enthalpy ratio vs mixing coefficient in the gridded bundle with the power distribution P7 and inlet temperature $T_{in} = 10°C$: (a) subchannel no. 7; (b) subchannel no. 8.

results in the gridded 7-rod bundle with uniform power distribution. Here, P is the bundle outlet pressure, G the bundle average mass flux, X_{in} the vapour quality at the inlet cross-section and Q the heating power.

Figure 6(a) and (b) show typical *CHF* results in dependence on the exit vapour quality of the hot subchannel at different mass fluxes G and pressures P. The data have been obtained in the gridded bundle [Fig. 6(a)] as well as in the wire wrapped bundle [Fig. 6(b)] with uniform radial power distribution. As expected, the *CHF* decreases with increasing vapour quality. Furthermore, the test data are proven to be well reproducible. It is seen that, at low vapour quality, *CHF* decreases with increasing pressure and decreasing mass flux, whereas at high vapour quality, an increase in *CHF* can be obtained by increasing pressure and decreasing mass flux. The influence of vapour quality, pressure and mass flux on *CHF* agrees well with that observed in circular tubes (Cheng et al., 1997).

Figure 7 compares the *CHF* values obtained in the bundle with wire wraps with those in the bundle with grid spacers. It is evident that the slope of the curve for the bundle with wire wraps is steeper than that for the bundle with grid spacers. Based on the subchannel conditions [Fig. 7(b)] both curves cross over at an exit vapour quality close to zero. For low vapour qualities, *CHF* of the bundle with wire wraps is higher compared to that of the bundle with grid spacers. An opposite influence of wire wraps on *CHF* is found for high vapour qualities. These results could be explained by the influence of wire wraps on local flow conditions near the wall in connection with flow-regime transition. At low vapour qualities with bubbly flow, wire wraps tend to enhance bubble transport from the heated wall and result in a higher *CHF*. At higher vapour qualities with annular flow, wire wraps tend to injure the liquid film on the heated surface and accelerate the dryout of the heated surface. Obviously, *CHF* correlations developed for gridded bundles cannot be directly applied to wire wrapped bundles.

Figure 8(a) and (b) show the *CHF* results obtained in the gridded bundle for four different radial power distributions. In all four cases, the heat flux is uniform on the surface which bounds the hot subchannel (no. 4). It is seen that for the conditions of these tests, *CHF* remains nearly unchanged at constant bundle inlet conditions. An analysis of the subchannel

Table 6
Some experimental results on *CHF* obtained in the gridded 7-rod bundle with uniform power distribution

P (MPa)	G (Mg/m^{2}s)	X_{in} (-)	Q (kW)	P (MPa)	G (Mg/m^{2}s)	X_{in} (-)	Q (kW)
2.98	5.946	−0.379	30.96	2.28	2.984	−0.820	45.54
3.00	5.932	−1.181	69.62	2.27	1.992	−0.128	14.27
3.00	3.953	−0.397	24.18	2.29	1.995	−0.869	34.22
3.00	3.993	−1.239	54.71	2.30	0.990	−0.250	11.67
2.99	2.977	−0.449	23.46	2.29	1.001	−0.929	22.71
2.96	2.999	−1.217	47.72	1.80	5.973	−0.156	25.38
2.99	1.990	−0.363	15.99	1.78	5.993	−0.570	58.86
3.01	2.000	−1.293	35.82	1.75	4.022	−0.097	19.84
3.00	1.021	−0.371	10.57	1.77	3.991	−0.587	46.75
3.00	0.993	−1.262	21.03	1.78	2.998	−0.149	20.38
2.73	5.740	−0.273	27.91	1.77	2.993	−0.603	41.02
2.73	5.900	−1.018	68.71	1.79	2.009	−0.142	16.69
2.75	3.858	−0.228	20.13	1.78	1.989	−0.652	32.63
2.73	3.956	−1.034	58.60	1.77	1.004	−0.155	12.74
2.72	2.987	−0.338	22.80	1.77	0.999	−0.689	21.17
2.71	2.983	−1.053	47.50	1.03	5.864	−0.132	26.51
2.73	1.982	−0.325	16.40	1.05	5.952	−0.325	44.32
2.74	1.996	−1.118	34.60	1.07	3.917	−0.102	21.86
2.76	1.032	−0.343	11.42	1.05	3.993	−0.344	38.76
2.70	1.012	−1.182	23.38	1.05	2.939	−0.083	19.53
2.31	5.831	−0.167	24.22	1.06	2.982	−0.357	34.88
2.28	5.946	−0.756	66.11	1.06	1.981	−0.079	18.51
2.32	3.956	−0.144	19.22	1.08	1.985	−0.374	28.33
2.28	3.964	−0.767	51.75	1.10	0.996	−0.087	14.75
2.28	2.969	−0.766	41.62	1.05	1.015	−0.403	22.65

flow conditions shows that the vapour quality and the mass flux in the hot subchannel decrease by increasing the number of the unheated rods. It is well known that a lower vapour quality leads to a higher *CHF*, whereas decreasing mass flux results in a reduction in *CHF*. Both effects compensate each other, so that the effect of the power distribution on *CHF* remains small. Based on subchannel conditions, a minor reduction in *CHF* is observed by changing the radial power distribution from uniform to non-uniform.

Figure 9(a) and (b) compare the *CHF* results obtained in the gridded bundle with uniform power distribution with those in bundles with five other non-uniform power distributions for which non-uniform heat flux distributions were achieved on the surfaces bounding the hot subchannel. *CHF* is plotted vs the bundle inlet conditions [Fig. 9(a)] as well as vs the subchannel conditions [Fig. 9(b)]. It is seen that, based on bundle inlet conditions, *CHF* in the bundle with uniform power distribution is lower than in bundles with non-uniform power distributions. By the transition from uniform to non-uniform power distribution, the effect of decreasing vapour quality is stronger than that of decreasing mass flux. Based on subchannel conditions, however, non-uniform power distributions result in a minor reduction in *CHF*.

Figure 10 compares the *CHF* results in the gridded 7-rod bundle with the data obtained in the 4.2 mm diameter tube (Cheng et al., 1997) which is comparable to the hydraulic diameter of the central subchannel (4.3 mm). The comparison is based on the direct substitution method

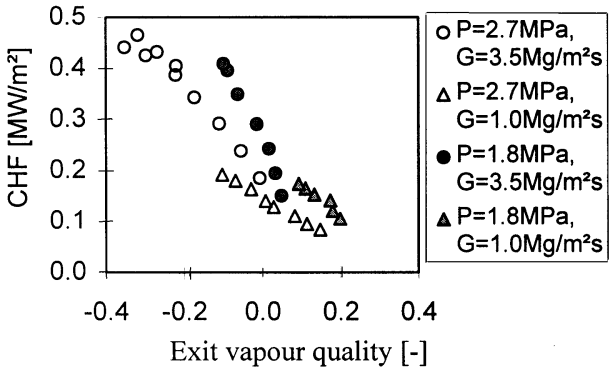

(a) 7-rod bundle with grid spacers

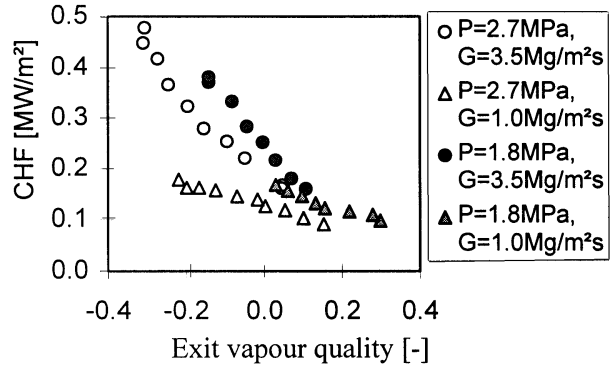

(b) 7-rod bundle with wire wraps

Fig. 6. Measured *CHF* in dependence on the subchannel conditions: (a) 7-rod bundle with grid spacers; (b) 7-rod bundle with wire wraps.

DSM (Siman-Tov, 1996). It is clearly seen that the *CHF* data in the 7-rod bundle are much lower than in the tube geometry. A larger deviation is observed at high pressures. This comparison underlines that *CHF* data obtained in circular tubes should not be applied directly to tight rod bundles.

Figure 11(a) and (b) compare the test results obtained in the gridded bundle of uniform power distribution with the *CHF* correlation GSM.6 which is valid for tight rod bundles and Freon-12. The ratio of the calculated *CHF* to the measured *CHF* is presented in dependence on pressure, mass flux [Fig. 11(a)] and local vapour quality [Fig. 11(b)]. On the average the GSM.6 correlation reproduces well the experimental data. The *CHF* ratio increases with increasing pressure and vapour quality. At high pressure or high vapour quality, the GSM.6 correlation overpredicts the test results, whereas at low pressure and low vapour quality the measured *CHF* is higher than the calculated one.

Figure 12(a) to (c) show the comparison of the test results with three different *CHF* prediction methods, all of which are only valid for water conditions. The comparison is based on the direct substitution method. To transfer the test results in Freon-12 to water conditions,

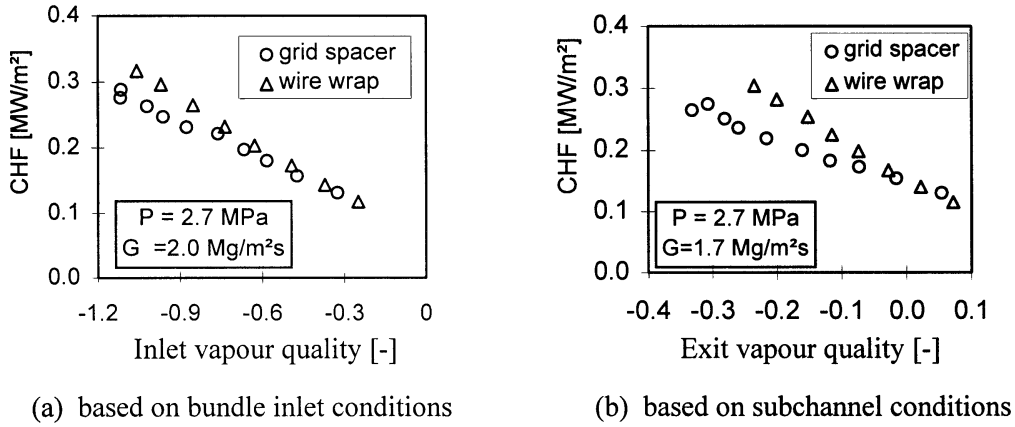

Fig. 7. Comparison of *CHF* results in the grided bundle with those in the wire wrapped bundle: (a) based on bundle inlet conditions; (b) based on subchannel conditions.

the fluid-to-fluid scaling law of Courtaud et al. (1988) has been used. A good agreement between the EPRI-1 correlation and the test data has been obtained at high pressures [Fig. 12(a)]. At low pressures the EPRI-1 correlation underestimates the test results significantly. Also, the KfK-3 correlation underestimates the experimental results at low pressures and low mass fluxes. At high pressures (≥2.3 MPa), a good agreement between the KfK-3 correlation and the test data is observed. The *CHF* look-up table overpredicts the measured *CHF* data in the tight rod bundle significantly [Fig. 12(c)]. Obviously, more accurate correction factors are needed to extend the application of the look-up table to tight rod bundle geometries.

Figure 13 compares the test results in the wire wrapped 7-rod bundle with uniform power distribution with the KfK-3 correlation which is the only one valid for rod bundles with wire wraps. Again, the comparison is based on the direct substitution method and the fluid-to-fluid scaling law of Courtaud et al. (1988). A good agreement between the experimental data and

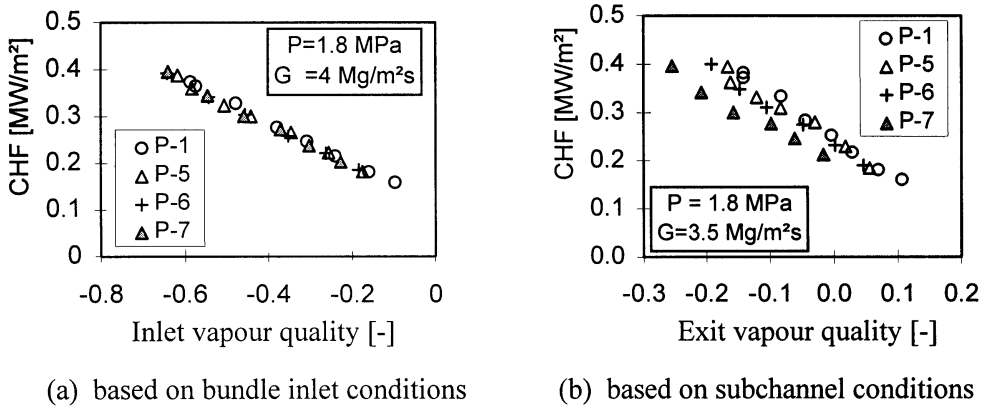

Fig. 8. *CHF* results in the gridded bundle of different radial power distributions with uniform heat flux on the hot subchannel surface: (a) based on bundle inlet conditions; (b) based on subchannel conditions.

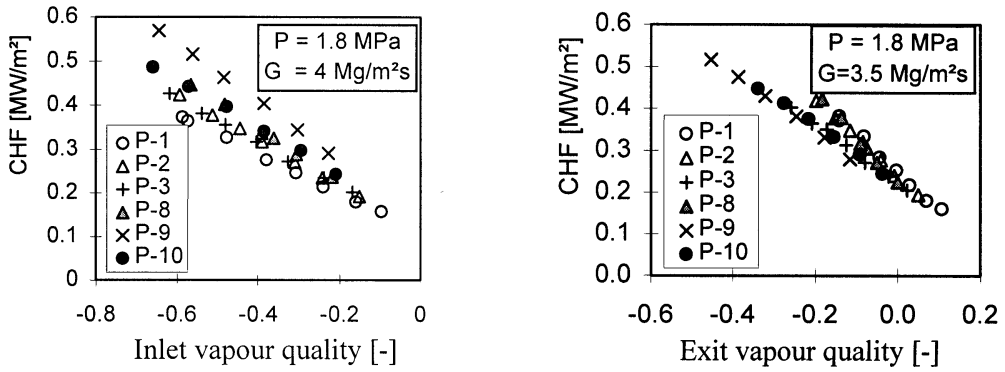

Fig. 9. *CHF* results in the gridded bundle for different radial power distributions with non-uniform heat flux on the hot subchannel surfaces: (a) based on bundle inlet conditions; (b) based on subchannel conditions.

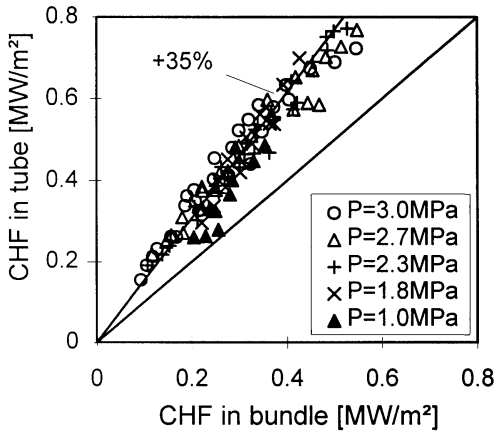

Fig. 10. Comparison of the test results in the gridded bundle with uniform power distribution with those in a circular tube of the same hydraulic diameter.

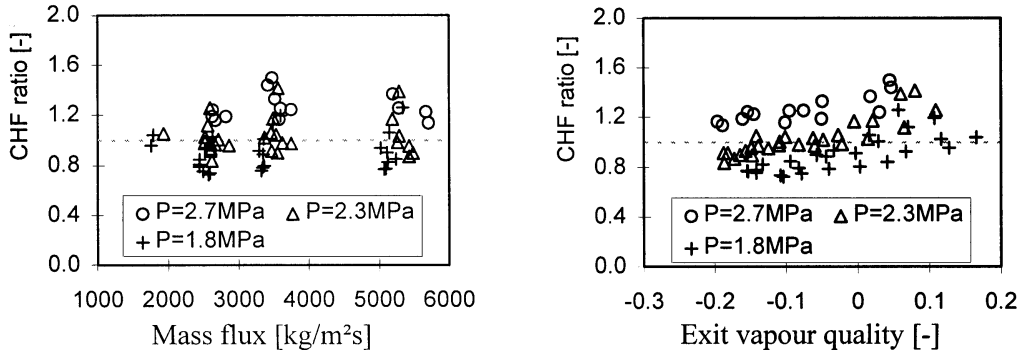

(a) in dependence on mass flux and pressure

(b) in dependence on exit vapour quality and pressure

Fig. 11. Comparison of the test results in the gridded bundle of uniform power distribution with the GSM.6 correlation: (a) in dependence on mass flux and pressure; (b) in dependence on exit vapour quality and pressure.

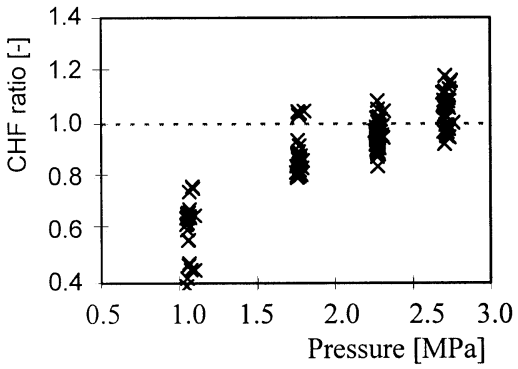

(a) EPRI-1 correlation of Fighetti et al. (1983)

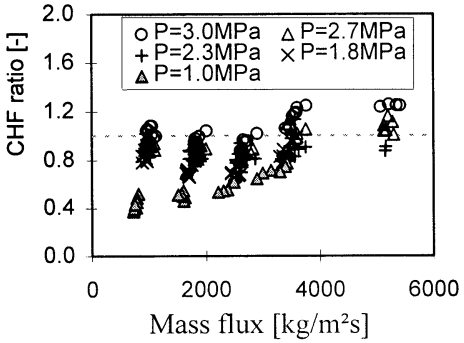

(b) KfK-3 correlation of Dalle-Donne (1991)

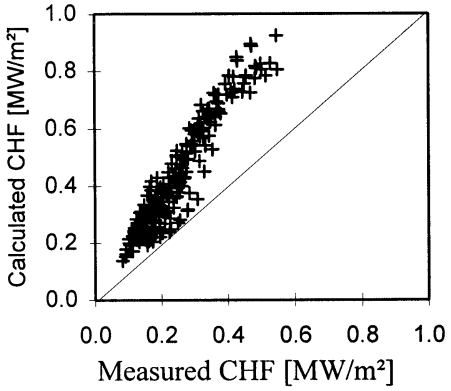

(c) CHF look-up table of Groeneveld et al. (1996)

Fig. 12. Comparison of the test results in the gridded bundle of uniform power distribution with different *CHF* prediction methods: (a) EPRI-I correlation of Fighetti et al. (1983); (b) KfK-3 correlation of Dalle-Donne (1991); (c) *CHF* look-up table of Groeneveld et al. (1996).

the KfK-3 correlation is obtained at low pressures (1.0 MPa). At high pressures, the KfK-3 correlation overpredicts the experimental results significantly.

5. Conclusion

In spite of a great quantity of experimental and theoretical studies of critical heat flux, knowledge of the precise nature of *CHF* is still incomplete. It is evident that for each specific design, experimental investigations should be performed and validated prediction methods must be derived. A detailed literature survey has indicated that experimental as well as theoretical works on *CHF* and turbulent mixing for tight hexagonal rod bundles under high

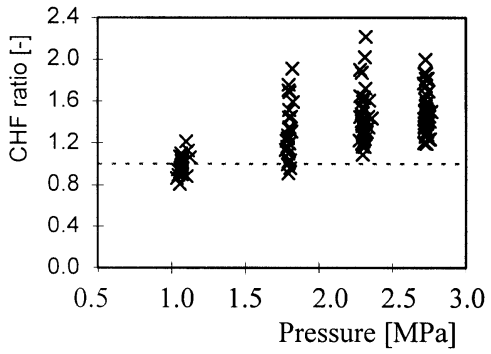

Fig. 13. Comparison of the test results in the wire wrapped bundle with uniform power distribution with the KfK-3 correlation of Dalle-Donne (1991).

pressures and high mass fluxes are scarce. In the present work investigations have been performed on critical heat flux and turbulent mixing in tight 7-rod bundles with different spacers and power distributions. Freon-12 was used as the working fluid due to its low latent heat, low critical pressure and well known properties. The main objectives of the present work were to supplement the *CHF* database available for rod bundles, especially for tight rod bundles, to analyse the effect of different parameters, e.g. wire wraps on *CHF*, to assess *CHF* prediction methods available and to investigate the turbulent mixing in tight rod bundles.

Based on the test data obtained and their analysis using the subchannel analysis code COBRA-IV, it has been found that the two-phase mixing coefficient depends mainly on mass flux. It increases with decreasing mass flux and ranges from 0.01 to 0.04 for the test condition considered. More than 900 *CHF* data points have been obtained in a large range of parameters: pressure 1.0–3.0 MPa and mass flux 1.0–6.0 Mg/m^2s. The effect of different parameters on *CHF* has been analysed. It has been found that the effect of pressure, mass flux and vapour quality on *CHF* is similar to that observed in circular tubes. Nevertheless, the *CHF* in the tight rod bundle is much lower than in a circular tube of the same equivalent hydraulic diameter. The *CHF* look-up table derived for circular tube geometries overpredicts the test results in the tight rod bundle significantly. The effect of wire wraps on *CHF* is mainly dependent on local vapour qualities and subsequently on flow regimes. At low vapour quality with bubbly flow wire wraps result in a higher *CHF*, whereas at high vapour quality with annular flow, wire wraps lead to a reduction in *CHF*. Based on subchannel flow conditions whose data are obtained using the COBRA-IV code and a constant mixing coefficient of 0.02, the effect of the radial as well as the circumferential heat flux distribution on *CHF* is small. Among the *CHF* correlations selected the GSM.6 correlation gives the best agreement with the test results.

Finally, it has to be pointed out that due to the large wall effect of the 7-rod bundles used, the applicability of the present results to a real tight fuel bundle needs further investigation. Therefore, experimental studies on *CHF* in a tight 37-rod bundle are performed at the Karlsruhe Research Center.

References

Bowring, R.W., 1979. WSC-2: A subchannel dryout correlation for water-cooled clusters over the pressure range 3.4–15.9 MPa. Winfrith: Atomic Energy Establishment, AEEW-R-983.

Cheng, X., 1991. Experimental investigations of critical heat flux in 8 mm tubes and in 7-rod bundles, KfK-report 4884. Research Center Karlsruhe.

Cheng, X., Erbacher, F.J., Müller, U., 1997. Critical heat flux in uniformly heated vertical tubes. Int. J. Heat Mass Transfer 40 (12), 2929–2939.

Courtaud, M., Deruaz, R., D'Aillon, L.G., 1988. The French thermal–hydraulic program addressing the requirements of the future pressurized water reactors. Nucl. Technol. 80, 73–82.

Dalle, Donne M., 1991. *CHF*-KfK-3: a critical heat flux correlation for triangular arrays of rods with tight lattices. Research Center Karlsruhe, KfK-4826.

Doroshchuk, V.E., Levitan, L., Lantsman, F.I., 1975. Recommendations for calculating burnout in a round tube with uniform heat release. Teploenergetik 22 (12), 66–70.

Fighetti, C.F., Reddy, D.G., 1983. A generalized subchannel *CHF* correlation for PWR and BWR fuel assemblies. Electric Power Research Institute, EPRI-NP-2609-Vol. 2.

Groeneveld, D.C., Cheng, S.C., Doan, T., 1986. 1986 AECL-UO critical heat flux look-up table. Heat Transfer Engineering 7 (12), 46–61.

Groeneveld, D.C. et al., 1996. The 1995 look-up table for critical heat flux in tubes. Nuclear Engineering and Design 163, 1–23.

Hewitt, G.F., Govan, A.H., 1990. Phenomena and prediction in annular two-phase flow. ASME Winter Annual Meeting, Dallas, pp. 41–56.

Katto, Y., Yokoya, S., 1987. Critical heat flux of forced convection boiling in uniformly heated vertical tubes with special reference to very large length-to-diameter ratios. Int. J. Heat Mass Transfer 30, 2261–2269.

Katto, Y., 1994. Critical heat flux. Int. J. Multiphase Flow 20 (Suppl.), 53–90.

Müller-Menzel, T., Zeggel, W., 1987. *CHF* in the parameter range of advanced pressurized water reactor cores. Nuclear Engineering and Design 90, 265–273.

Oldekop, W., Berger, H.D., Zeggel, W., 1982. General features of advanced pressurized water reactors with improved fuel utilization. Nucl. Technol. 59, 212–227.

Rehme, K., 1973. Pressure drop correlations for fuel element spacers. Nucl. Technol. 17, 15–23.

Rogers, J.T., Rosehart, R.G., 1972. Mixing by turbulent interchange in fuel bundles, correlations and inferences. ASME-Paper-72-HT-53.

Rowe, D.S., Johnson, B.M., 1974. Implications concerning rod bundle crossflow mixing based on measurements of turbulent flow structure. Int. J. Heat Mass Transfer 17, 407–419.

Siman-Tov, M., 1996. Application of energy balance and direct substitution methods for thermal margins and data evaluation. Nucl. Engng Des. 163, 249–258.

Todreas, N.E., Rogers, J.T., 1976. Coolant interchannel mixing in reactor fuel rod bundles single-phase coolants. The Winter Annual Meeting of ASME, New York, pp. 1–56.

Tong, L.S., Hewitt, G.F., 1972. Overall viewpoint of flow boiling *CHF* mechanisms. ASME paper 72-HT-54.

Weisman, J., Ying, S.H., 1985. A theoretically based critical heat flux prediction for rod bundles at PWR conditions. Nucl. Engng Des. 85, 239–250.

Wheeler, C.L., Stewart, C.W., Cena, R.J., Rowe, D.S., Sutey, A.M., 1976. COBRA-IV–I: an interim version of COBRA for thermal–hydraulic analysis of rod bundle nuclear fuel elements and cores. Battelle, Pacific Northwest Laboratories, Richland, Washington, BNWL-1962, UC-32.

Wolf, L., Fischer, K., Herkenrath, H., Hufschmidt, W., 1987. Comprehensive assessment of the ISPRA BWR and PWR subchannel experiments and code analysis with different two-phase models and solution schemes. Nucl. Engng Des. 99, 329–350.